2017

Using Low-Coherence Interferometry to Monitor Cell Invasion in an in-vitro Model System

Behnaz Davoudi Nasab
University of Central Florida

USING LOW-COHERENCE INTERFEROMETRY TO MONITOR CELL INVASION IN AN *IN-VITRO* MODEL SYSTEM

by

BEHNAZ DAVOUDI NASAB

A thesis submitted in partial fulfillment of the requirements
for the Honors in the Major Program in Chemistry
in the College of Sciences
and in the Burnett Honors College
at the University of Central Florida
Orlando, Florida

Spring Term 2017

Thesis Chair: Dr. Aristide Dogariu

ABSTRACT

In an optically random system, such as naturally occurring and man-made media, light undergoes pronounced multiple scattering. This phenomenon has shown a remarkable potential in characterizing complex materials. In this regime, scattering occurs from each individual center of the scattering and independent scattering events lead to multiple light scattering. This phenomenon is often described as a random walk of photons and can be modeled in terms of a diffusion equation based on the radiative transfer theory. In this thesis, we used optical path-length spectroscopy (OPS), which is an experimental method to obtain the path-length probability density of the propagating light in multiple scattering media, with a low-coherence optical field to investigate the distribution of photon path lengths in a skin cell model system. This method is capable of measuring the transport mean free path of light in a highly scattering medium and depth-resolved profiles of the backscattered light. Our OPS experimental configuration is based on a fiber-optic Michelson interferometer geometry using single mode optical fibers. We performed OPS based on low-coherence interferometry (LCI) on three-dimensional organotypic models of esophageal cell invasion by measuring the optical path-length distribution of backscattered light in normal and invasive conditions. The optical path-length distribution of light waves inside the cell samples provides information on how a change in the extracellular matrix affects invasiveness of the esophageal cells and induction of signaling pathways. Also, we demonstrated the compatibility to study the structural changes during a two-week period for in vitro cell samples.

This thesis is dedicated to my incredible parents, Javad and Soheila,
to my wonderful boyfriend, Sepehr
and in loving memory of my brother, Behzad.

ACKNOWLEDGMENTS

I would like to thank my advisor, Dr. Aristide Dogariu for all his continued supports, and for giving me the opportunity to work in CREOL as an undergraduate research assistant. Working in CREOL helps me to build my knowledge in Optics, my technical skills in lab, and my confidence in research areas in addition to my major, Chemistry. Research experience in my undergraduate provided me a unique opportunity to explore my options for graduate studies.

I would like to thank Dr. Claudia Andl and her research group specially Gregoire, our collaborators in the Burnett School of Biomedical Science at the University of Central Florida. Dr. Andl prepared the samples for us and helped me in learning and understanding the biology part of our research without any hesitation.

I would like to express my gratitude to each and every one of my group members in Photonics Diagnostic of Random Media group for being supportive and fun to work with specially Roxana for being a wonderful mentor.

Most importantly, I would like to thank my family, my mother, my father, and my brother for their continuous love, support, encouragement, and believe that they always had in me. I would specially like to thank my boyfriend, Sepehr, for standing beside me and always inspiring me when I feel hopeless. Also, I would like to thank Golnaz, my best friend and my sister through years, for her unconditional love and support. My thesis would not have been possible without their love and support.

TABLE OF CONTENTS

LIST OF FIGURES vii

LIST OF TABLES ix

CHAPTER 1: INTRODUCTION 1

CHAPTER 2: OPTICAL INTERACTIONS IN INHOMOGENEOUS MEDIA 4

2.1. Electromagnetic Waves 5

2.2. Scattering of Electromagnetic Waves 7

2.2.1. Scattering from a single dielectric particle 7

2.2.2. Light-matter interaction in inhomogeneous medium 8

CHAPTER 3: EXPERIMENTAL TECHNIQUES 13

3.1. Theory of optical interference 13

3.1.1. Michelson interferometry with low-coherence fields 15

3.2. Optical path-length spectroscopy 17

CHAPTER 4: EXPERIMENTS ON AN IN-VITRO MODEL SYSTEM OF ESOPHAGUS TISSUE 21

4.1. Model system of Esophageal tissues 21

4.2. Precision Reflectometry 25

4.2.1. Experiments on esophageal tissue samples 28

4.2.2. Results and discussions 30

CHAPTER 5: CONCLUSIONS 38

LIST OF REFERENCES 39

LIST OF FIGURES

Figure 2-1: Scattering of light from a single dielectric particle 7

Figure 2-2 Scattering regimes in different conditions 9

Figure 2-3 Scattering trajectory in a random media 10

Figure 3-1 Schematics of Michelson interferometer 16

Figure 3-2 Experimental setup for a LCI based backscattering OPS 18

Figure 3-3 Measured path-length distribution vs optical path-length by using OPS method 20

Figure 4-1 The transforming growth factor β (TGFβ) signaling pathway [30] 23

Figure 4-2 Molecular structuer of A83-01[30] 24

Figure 4-3 Effect of TGFβR inhibitor in a normal tissue and high colagen density tissue (from Andl Lab in the Burnett School of Biomedical Science at the University of Central Florida) 25

Figure 4-4 Agilent HP 8504B 1300-1550 nm precision reflectometer 26

Figure 4-5 Layers of an optical fiber, tools for cleaving process 27

Figure 4-6 DC power supply and light source controller 28

Figure 4-7 Esophageal tissue samples and the reflectometer instrument, OPS measurements were performed with single mode optical fibers 28

Figure 4-8 The preliminary signal observed from the sample 29

Figure 4-9 The measured OPS signal when the fiber tip is touching the epithelium layer ... 30

Figure 4-10 Protocol for growing the organotypic model systems (from Andl Lab in the Burnett School of Biomedical Science at the University of Central Florida) 31

Figure 4-11 Measured path length distributions for cultures in normal condition in the presence and absence of fibroblasts in several days after embedding epithelial cells..... 31
Figure 4-12 A) H&E of Cellular matrix with high collagen density in absence of TGFβR inhibitor (low invasion) B) H&E of Cellular matrix with high collagen density and TGFβR inhibitor (medium invasion), (from Andl Lab in the Burnett School of Biomedical Science at the University of Central Florida)..... 32
Figure 4-13 Measured $P(\boldsymbol{s})$ vs optical path-length ($\boldsymbol{s}$) for low invasion, and medium invasion samples in logarithmic scales during different days (a) 4 days after embedding epithelial cells, (b) 7 days after embedding epithelial cells, and (c) 9 days after embedding epithelial cells 33
Figure 4-14 H&E of Cellular matrix with high collagen density in absence of TGFβR inhibitor (low invasion) B) H&E of Cellular matrix with high collagen density and TGFβR inhibitor (medium invasion) C) H&E of Cellular matrix with low collagen density in absence of TGFβR inhibitor (high invasion), (prepared in Andl's Lab in the Burnett School of Biomedical Science at the University of Central Florida)..... 34
Figure 4-15 OPS measurements on low invasion, medium invasion, and high invasion in different days, (a) 5 days after embedding epithelial cells, (b) 7 days after embedding epithelial cells, (c) 8 days after embedding epithelial cells, (d) 9 days after embedding epithelial cells 35
Figure 4-16 Averaged measurements on 50 different points on the sample for three different conditions, (a) Low Invasion, (b) Medium Invasion, (c) High Invasion, shown in logarithmic scales with a linear fit 36
Figure 4-17 Structural properties of investigated three different conditions..... 37

LIST OF TABLES

Table 4-1 Area Under the graph from 10 μm to 500μm $(\times 10 - 4)$..... 36

CHAPTER 1: INTRODUCTION

Light as an electromagnetic wave shows wave-like properties such as reflection, refraction, scattering, and interference. Electromagnetic wave plays a vital role in probing the structural properties and dynamics of materials. For example, information about the absorption of different wavelengths reveals detailed understanding about electronic, vibrational, and rotational energy levels of molecules and helps chemists and physicists to study the structural configuration of complex molecules. Spectroscopic observations have had a remarkable impact on different aspects of physical sciences such as solid-state and molecular physics, organic, and inorganic chemistry. Within the scope of light-matter interaction, a group of phenomena arises from processes that light undergoes. Among them, wave scattering by particles is of great interest and can be characterized by the scattering phenomenon of light. When light shines on the matter, the electric field generates an oscillating polarization of the electrons which results in a secondary source and subsequently radiates light. This radiation depends on the structure of the scattering material and provides information about the geometry of the medium. The basis of scattering was predicted a long time ago by Rayleigh, Mie, and other experts in this field and recent developments in laser have helped to understand it experimentally in different frameworks. Another phenomenon that is well-known in everyday life is interference of two or multiple waves which can generate bright and dark fringes in the resultant interference pattern. An example of this is the ocean where water waves are generating patterns. In optical sciences, the interference of two light waves in the double-slit experiment is a proof that light can be described as a wave. The generation of interference patterns is utilized in modern experimental apparatus where the interest is to characterize the

properties of the phase of the electromagnetic waves. This is based on the ability of interference to translate the information from phase into the detected intensity [1].

Unexpected behavior happens when light interacts with heterogeneous media that cannot be predicted by assuming a simple light-matter interaction picture, and it requires understanding the interaction in a complex system. The interaction of light with complex systems has attracted attention in different applications such as material characterization, medicine, chemistry, and biology. In 1976, Goodman observed that when a coherent continuous wave laser beam is reflected from a rough surface a speckle pattern with spatial fluctuations is formed [2]. The origin of this random distribution is the surface roughness which is comparable with the wavelength. As an illustrative example, consider a paper sheet with three-dimensional stochastic networks of fibers [3]. The complex composition of a paper sheet causes multiple scattering events and interferences which can be modeled by different approaches. One approach is based on direct use of Maxwell's equations and solving it for simplified model of paper and calculating the superposition of scattered intensities [4]. This approach provides information about the material properties such as scattering cross-section and absorption but lack the real interaction picture and actual light scattering phenomena. In order to have a detailed understanding of the light-matter interaction, it is required to exactly know the structure of the medium and model the scattering as a complex process which is not possible in most cases.

The motivation of this work is to use low-coherence interferometry, which is a well-known experimental technique, to study a model system of an inhomogeneous medium where light experiences multiple scattering. The backscattered light from this complex system is

studied by optical path-length spectroscopy to model the light-matter interaction and study the structural properties of the medium. This research has been done in collaboration with Dr. Claudia Andl's group in the Burnett School of Biomedical Science at the University of Central Florida. We studied a tissue model of esophageal cells to monitor the contributing effect on the cell invasion. The models are grown in Dr. Andl's laboratory as organotypic cultures. The tumor microenvironment contributes to cell invasion through reorganization of the extracellular matrix and induction of signaling pathways. Our goal is to monitor the cell invasion by using OPS technique [5].

The thesis is organized as follows. A brief theoretical background and formalism of multiple light scattering phenomenon needed for this thesis, particularly focusing on optical path-length probability density and its modeling based on a random walk of photons, is presented in Chapter 2. In Chapter 3, the basic optical interferometric background used in experimental work of this thesis is introduced. This includes discussions on the principles of Michelson interferometry for a partially coherent light and the experimental apparatus for measuring the optical-path length distribution. Chapter 4 starts with an overview of the model systems studied in this thesis. The second part introduces the methodology to determine the optical path-length probability density of three-dimensional models of esophageal cell and the discussion on the results to study the effects of changes in the extracellular matrix on invasiveness and the induction signaling pathways. Chapter 5 gives conclusions of this thesis and discusses possible future research.

CHAPTER 2: OPTICAL INTERACTIONS IN INHOMOGENEOUS MEDIA

Light as an electromagnetic wave can be described by similar rules governing all forms of electromagnetic radiation. There are different approaches to approximate the way of treating light depending on the size of the objects in the surrounding media of the light. For objects with much greater dimensions than the wavelength, the interaction can be adequately described by ray optics which is mainly concerned with the location and direction of light rays. As the size of the objects become smaller, ray optics approximation will not be useful anymore and the wave properties of light obeying electromagnetic theory will be more pronounced. This will open a class of interesting phenomena of light-matter interaction such as interference, optical coherence, light scattering, and etc. When light experiences materials with complex structures, it undergoes unpredictable fluctuations in which case requires more complicated analysis to understand the interaction. Controlling the degree of coherence of light provides unique characteristics and opens new possibilities for monitoring the light-matter interaction in materials with inhomogeneous structures.

This chapter provides a basic classical approach for describing the interaction between light and matter, where, the medium is optically inhomogeneous. In this work, we will primarily focus on understanding the concept of multiple light scattering, originating from the complex interaction of light with matter. To describe them, basic fundamentals of electromagnetic waves are introduced. Some wave-like properties of light such as scattering from a simple dielectric particle and multiple light scattering are discussed. In addition, the

propagation of light in such a media is modeled based on a random walk description and a diffusion approximation to the radiative transfer theory.

2.1. Electromagnetic Waves

The principles of electromagnetic waves can be described by Maxwell's equations. In general, the electromagnetic wave is formed by two related vector fields, the electric field, $\vec{E}(\vec{r},t)$, and the magnetic field , $\vec{H}(\vec{r},t)$. These vector fields are both a function of position, $\vec{r}$, and a given point in time,t, that are orthogonal to each other in space. In a source free region (a medium with no charges) and non-magnetic medium, the electric field and magnetic field are related to electric flux density, $\vec{D}(\vec{r},t)$, and magnetic flux density, $\vec{B}(\vec{r},t)$, through constitutive relations as below:

$$\vec{\boldsymbol{D}}(\vec{\boldsymbol{r}},\boldsymbol{t}) = \boldsymbol{\varepsilon}\vec{\boldsymbol{E}}(\vec{\boldsymbol{r}},\boldsymbol{t}) \quad \textbf{(2-1)}$$

$$\vec{\boldsymbol{B}}(\vec{\boldsymbol{r}},\boldsymbol{t}) = \boldsymbol{\mu_0}\vec{\boldsymbol{H}}(\vec{\boldsymbol{r}},\boldsymbol{t}), \quad \textbf{(2-2)}$$

where ε is the electric permittivity of the medium and μ_0 is the vacuum permeability and its value is $\mu_0 = 4\pi \times 10^{-7} H.m^{-1}$. For a source-free region, the Maxwell's equations governing the mentioned time-harmonic field vectors are

$$\vec{\boldsymbol{\nabla}} \times \vec{\boldsymbol{E}}(\vec{\boldsymbol{r}},\boldsymbol{t}) = -\frac{\boldsymbol{\partial}}{\boldsymbol{\partial t}}\vec{\boldsymbol{B}}(\vec{\boldsymbol{r}},\boldsymbol{t}) \quad \textbf{(2-3)}$$

$$\vec{\boldsymbol{\nabla}} \times \vec{\boldsymbol{H}}(\vec{\boldsymbol{r}},\boldsymbol{t}) = \frac{\boldsymbol{\partial}}{\boldsymbol{\partial t}}\vec{\boldsymbol{D}}(\vec{\boldsymbol{r}},\boldsymbol{t}) \quad \textbf{(2-4)}$$

$$\vec{\boldsymbol{\nabla}}.\vec{\boldsymbol{D}}(\vec{\boldsymbol{r}},\boldsymbol{t}) = \boldsymbol{0} \quad \textbf{(2-5)}$$

$$\vec{\boldsymbol{\nabla}}.\vec{\boldsymbol{B}}(\vec{\boldsymbol{r}},\boldsymbol{t}) = \boldsymbol{0}. \quad \textbf{(2-6)}$$

In general, the vector fields can be described in a spatial coordinate system in which case Maxwell's equations provide the time and position dependent changes of three scalar functions for each of the vector fields. We use the term wave to denote a solution to a particular type of equation, which is called wave equation. In order to understand the wave-like properties of these vector fields, it is necessary to solve the wave equation governing on each of these scalar functions. By taking the curl of the equation (2-3) and substituting $\vec{\nabla} \times \vec{H}(\vec{r}, t)$ from equation (2-4), and using the $\vec{\nabla} \times \left(\vec{\nabla} \times \vec{E}\right) = \vec{\nabla}\left(\vec{\nabla}.\vec{E}\right) - \nabla^2\vec{E}$ identity, the wave equation becomes:

$$\nabla^2\vec{E} - \frac{1}{c^2}\frac{\partial^2}{\partial t^2}\vec{E} = 0 \qquad \textbf{(2-7)}$$

The similar equation also governs the magnetic vector field. This type of wave equation is valid for a source free and isotropic medium. For a homogeneous medium, the solution of the wave equation follows a special case which is called plane waves. This solution is forming the eigenfunctions of the wave equation's vector space. By solving the partial differential equation of 2-7, the exponential plane wave solutions become

$$\vec{E}(\vec{r}, t) = \vec{E}_0 e^{-i(\vec{k}.\vec{r} - \omega t)} \qquad \textbf{(2-8)}$$

$$\vec{H}(\vec{r}, t) = \vec{H}_0 e^{-i(\vec{k}.\vec{r} - \omega t)}, \qquad \textbf{(2-9)}$$

where $\vec{E}_0$ and $\vec{H}_0$ are showing the amplitude and polarization of the electric and magnetic fields, respectively, and are orthogonal to each other, $\vec{k}$ is the wavevector with a magnitude of $n\frac{\omega}{c}$ parallel to the direction of propagation, and ω is the oscillating frequency of the electromagnetic wave. In the presence of a particle in the medium, the propagation of the wave should be analyzed with scattering theory.

2.2. Scattering of Electromagnetic Waves

Scattering is a physical process that initiates from the collision between the wave energy and particles inside the medium. To examine how the electromagnetic field interacts with a medium consisting scattering particles, we will discuss the principles of scattering from a single particle and more complex systems in the next section.

2.2.1. Scattering from a single dielectric particle

Let us consider a medium with a particle whose dielectric optical properties are different that the surrounding region. The simplest case is when a particle with an arbitrary shape and size is assumed by a complex relative electric permittivity as below:

$$\varepsilon_r(\vec{r}) = Re\{\varepsilon_r\} + iIm\{\varepsilon_r\} \quad \textbf{(2-10)}$$

The complex nature of the relative permittivity reveals information on the refractive properties and loss of the scattering medium. The general case of a scatterer is assumed by having a relative permittivity, ε_r, which depends on position for a static case. As shown in Figure 2-1, the incident linearly polarized plane wave on the scatterer is given by $\vec{E}_i$ and the scattered light is given by $\vec{E}_s$ which can obtain a non-planar wavefront.

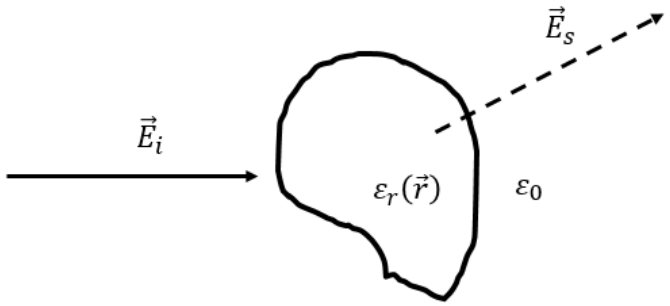

Figure 2-1: Scattering of light from a single dielectric particle

The scattering event can be characterized by the scattering cross-section which is defined as

$$\sigma_d(\vec{k}_i, \vec{k}_s) = \left|g(\vec{k}_i, \vec{k}_s)\right|^2 \quad \textbf{(2-11)}$$

where $\vec{k}_i$ is the wavevector of the incident plane wave and $\vec{k}_s$ is the wavevector of the scattered light. The function $g(\vec{k}_i, \vec{k}_s)$ depends on the characteristics of the scattering process and shows the amplitude, phase and polarization of $\vec{E}_s$. By having $\vec{k}_s = -\vec{k}_i$ the measured cross-section corresponds to the backscattering events. This explanation is for a general particle with a given size and shape. Scattering from particles with much smaller size than the wavelength is called Rayleigh scattering. In this case the field inside the particle can be approximated as uniform and the scattering radiation pattern follows a small dipole. The exact analysis of scattering for a homogeneous and isotropic spherical particle was done by Mie in 1908. More complex geometries require a complicated mathematical analysis which is not in the scope of this thesis. In practical situations, the scattering medium includes numerous scattering particles, therefore, the superposition of scattering events from individual center of the particles contributes to the scattered light. This leads to multiple light scattering which will be discussed in the next section.

2.2.2. Light-matter interaction in inhomogeneous medium

An inhomogeneous medium such as solutions of biological macromolecules, molecular fluids, electrolyte solutions, colloidal suspensions, and biological tissues have granted attention in optical sciences and have been studied by using laser sources. In an optically inhomogeneous system, the incident monochromatic light undergoes pronounced multiple scattering.

The interaction of light with a disordered medium has been historically considered as a great inconvenience, however, disordered structures have been recently proved to offer a wealth of important application in different areas [6]. Different scattering regimes can take place depending on the propagation of light through different concentration of particles in an inhomogeneous system. In a random system with a low concentration of particles, the incident light undergoes a single scattering event prior to detection which is known as single scattering regime and is shown in Figure 2-2. Moreover, multiple scattering regime occurs in a medium with a higher concentration of scattering particles in which the incident light will be scattered multiple times. As the concentration of particles increases, the distance between the particles decreases, and as a result, the group of scattering particles may behave as a single scatterer. In such a circumstance, the collective scattering regime takes place (Figure 2-2). In this thesis, we will focus mostly on multiple scattering regimes.

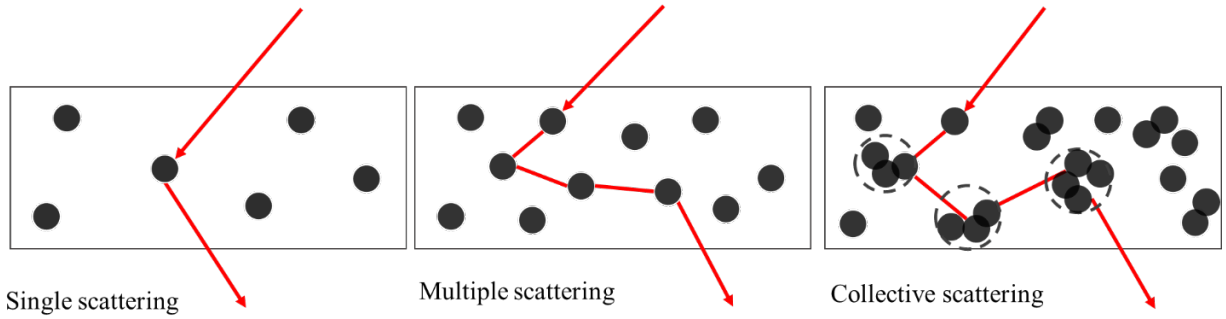

Figure 2-2 Scattering regimes in different conditions

In multiple scattering regimes, the field energy that is traveling through the inhomogeneous media can be characterized by different parameters as shown in Figure 2-3, where L is the thickness, l_s is a global parameter called scattering mean free path (the average

distance between two scatterers), and l_t is the transport mean free path (the average distance which the directional energy flux is randomized through sequential scattering events).

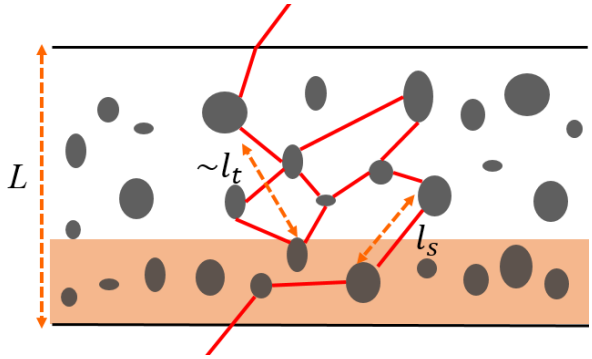

Figure 2-3 Scattering trajectory in a random media

In such systems, the total number of scattering events can be estimated as the number of scattering event times the scattering mean free path.

$$\boldsymbol{s = l_s . n} \tag{2-12}$$

where l_s is inversely proportional to the scattering coefficient μ_s, and n is the number of scattering events that are happening in the random system. The scattering mean free path l_s due to the propagation of light in a scattering medium can be obtained from the following

$$\boldsymbol{l_s = \frac{1}{N\sigma}} \tag{2-13}$$

in which N stands for number density of scattering particles and σ for the total extinction cross section of one scattering event which is estimated as:

$$\boldsymbol{\sigma = \sigma_s + \sigma_a} \tag{2-14}$$

where σ_s stands for scattering cross section of a single scattering event and σ_a stands for the absorption cross section of a single scattering event in which case for our measurements σ_a is neglected due to the absence of absorption. The optical transmission is commonly considered

as anisotropic scattering in which the transport mean free path can be obtained from the scattering mean free path.

$$l_t = \frac{l_s}{(1-g)} \tag{2-15}$$

where g is scattering anisotropy factor. The equation 2-13 and equation (2-15) can be arranged to give the following:

$$l_t = \frac{1}{N\sigma_s(1-g)} \tag{2-16}$$

The residual non-scattered power is found based on the Beer-Lambert law for the total input power of P_0 as

$$P = P_0 exp^{\frac{-L}{l_s}} \tag{2-17}$$

In practical applications solving the scattering problem analytically means to characterize the scattering events in detail and requires exact information about the structure of the medium. One method to study the geometry of the scattering medium is to solve the inverse scattering problem which means finding information about the medium by using the properties of the scattered light. For a highly scattering medium, the radiative transport theory works well which can be described based on a random walk of photons and modeled after the diffusion approximation [7]. This approach deals with the propagation of the distribution of energy inside the medium. For the portion of the wave that is transported into a diffusive scattering medium, the governing equation for the diffuse energy density, $\psi(\vec{r},t)$, is

$$\frac{\partial\psi(\vec{r},t)}{\partial t} - D\nabla^2\psi(\vec{r},t) = \delta(\vec{r})\delta(t) \tag{2-18}$$

where $\delta(\vec{r})$ and $\delta(t)$ are the impulse sources respectively, and D is the diffusion coefficient of photons in the medium which provides information about the scattering medium, and is given by

$$D = v\frac{l_t}{3} \quad \textbf{(2-19)}$$

where v is the speed of energy transport.

Solving this equation by considering appropriate boundary condition yields to the energy flux inside the scattering medium [8]. The energy flux shows a dependency on the traveled optical path-length, s. In normal diffusion regime, the path-length distribution decays as a power law with a $-5/2$ exponent [5]. A diffusion equation gives an approximation of the energy that is transported through the system with the assumption that the velocity is constant through an isotropic elastic scattering and wave propagation. In this case, the wave properties of light are disregarded [9]. For many realizations of disorder, different diffusive regimes may occur [10]. There are different characterization techniques to fully understand how light-matter interaction evolves in disordered structures [11].

In the next chapter, we will present the basics of optical interference required for understanding the techniques that we used to extract the information on the multiple scattering medium and we will explain the working principle of our experimental technique and the results.

CHAPTER 3: EXPERIMENTAL TECHNIQUES

This chapter provides an introduction to experimental techniques used within the scope of this work. First, we explain how plane waves interfere with each other which is the principle of the interferometric devices such as Michelson interferometer, Sagnac interferometry, and Mach-Zehnder configurations. In the second section, the Michelson interferometer for a partially coherent light is explained and subsequently, the LCI method by using the OPS technique for the backscattered light is presented.

3.1. Theory of optical interference

The optical interferometry has been developed over more than 300 years in parallel to the history of wave optics [1]. There are different optical devices that are working based on optical interference. For example, optical coherence tomography (OCT) is a popular technique in different biomedical applications such as biomedical imaging, optical biopsy [12], and etc. The main advantage of OCT is the high resolution and its ability to capture cross sectional tomographic images from highly dense layered media especially in biological tissues [13].

To understand how interferometer works, first we need to explain the basic principle behind the optical interference. For simplifying the analysis, let us consider two plane waves with different amplitudes, same frequencies, and both having parallel polarizations along $\hat{u}$ that are propagating in two different directions such as:

$$\vec{E}_1(\vec{r},t) = \hat{u}E_{01}e^{-i(\vec{k}_1.\vec{r}_1-\omega t)} \quad \textbf{(3-1)}$$

$$\vec{E}_2(\vec{r},t) = \hat{u}E_{02}e^{-i(\vec{k}_2.\vec{r}_2-\omega t)} \quad \textbf{(3-2)}$$

The intensity of the individual electric fields can be defined as

$$I_1(\vec{r},t) = \vec{E}_1.\vec{E}_1^{\,*} = \left|\vec{E}_1\right|^2 \quad \textbf{(3-3)}$$

$$I_2(\vec{r},t) = \vec{E}_2.\vec{E}_2^{\,*} = \left|\vec{E}_2\right|^2 \quad \textbf{(3-4)}$$

The intensity can be measured by commercial detectors. However, more complicated methods are required to measure the phase information of the field. Interference has the ability to translate this information into the measured intensity. When two plane waves superimpose each other, the phase difference between them plays an important role in the total intensity. The total electric field is

$$\vec{E}(\vec{r},t) = \vec{E}_1(\vec{r},t) + \vec{E}_2(\vec{r},t) = \hat{u}(E_{01}e^{-i(\vec{k}_1.\vec{r}_1-\omega t)} + E_{02}e^{-i(\vec{k}_2.\vec{r}_2-\omega t)}) \quad \textbf{(3-5)}$$

Therefore, the total intensity will be

$$I(\vec{r},t) = \vec{E}.\vec{E}^* = I_1(\vec{r},t) + I_2(\vec{r},t) + 2Re(E_{01}E_{02}e^{-i(\vec{k}_2\vec{r}_2-\vec{k}_1\vec{r}_1)}) \quad \textbf{(3-6)}$$

The interference pattern is the equation of the locus of the bright fringes of irradiance which happens when the intensity becomes maximum or $\vec{k}_2\vec{r}_2 - \vec{k}_1\vec{r}_1 = 2\pi m$, where m is an integer. This equation also represents the trajectory of bright fringes in which case for plane waves becomes straight and equally spaced lines in the Cartesian coordinates. In general, the interference pattern depends on the number of interfering waves, spatial distribution, and the wavefront. For example, for spherical waves the equation of the wavefront will be different and the shape of the fringes observed on an arbitrary observation plane depends on where the detection screen is placed.

Among the optical interferometry techniques, Michelson interferometer has received significant attention due to its applications in precise measurements of length [14], optical testing [15], stellar interferometry [16], and recently in Laser Interferometer Gravitational-

Wave Observatory (LIGO) project [17]. We will explain the principles of partially coherent Michelson interferometer in the next section.

3.1.1. Michelson interferometry with low-coherence fields

For a monochromatic plane wave, if we know the electric field at a given time and position, we can anticipate its behavior. In real life, the ensemble averages of measurable quantities are of interest because instead of deterministic or "coherent" monochromatic plane waves, there are disturbances of fluctuations of wave in time and space. The theory of optical coherence studies these random fluctuations. In random light, the dependence of the wave is not predictable. Therefore, the measurable quantity will be a random process. In statistical optics, light can be categorized to coherent, incoherent, or partially coherent waves. The parameters describing the properties of random light have to be explained as an average over an ensemble of random processes. For example, the optical intensity can be described as $\langle|\vec{V}(\vec{r},t)|^2\rangle$, where $\vec{V}$ is the field disturbance in a given point in space and time. The ability of light to interfere with a temporally delayed version of itself, at a fixed position, is called temporal coherence. Similar definition is also valid for spatial coherence.

In 1881, Albert Michelson developed the Michelson interferometer. This method has attracted a significant attention in high precision measurements, modern physics, and biomedical applications. The working principle of Michelson interferometer is based on the interference between two waves that one of them is acting as a reference and the other one is interacting with the Device Under Test (DUT). In general, Michelson interferometer consists of two arms (Figure 3-1), light from a source S is divided into two beams with a beam-splitter and they are reflected back at two mirrors M_1 and M_2. M_1 is an adjustable mirror which is

placed in the reference arm and enables micrometer control of the optical path-length and the sample is placed in the other arm which interacts with the beam two times before and after reflection from M_2.

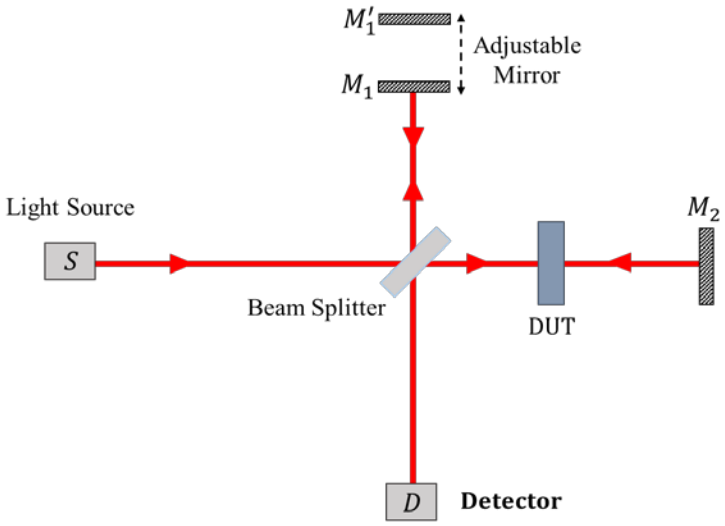

Figure 3-1 Schematics of Michelson interferometer

The total electric field captured by the detector is given by:

$$V(t) = V_1(t - t_1) + V_2(t - t_2) \tag{3-7}$$

where V_1 is the spatially coherent electric field disturbance of light in one arm with the temporal delay of t_1 and V_2 is the electric field disturbance in the second arm with the temporal delay of t_2. The total intensity detected by the detector is written as following:

$$I(t) = \langle V(t)V(t)^* \rangle \tag{3-8}$$

where * represents as the conjugation of electric field. The total intensity can be also rewritten as:

$$I(t) = I_1(t) + I_2(t) + 2Re[\Gamma(t - t_1, t - t_2)] \tag{3-9}$$

where $\Gamma(t_1, t_2)$ is shown as following

$$\Gamma(t_1, t_2) = \langle V_1^*(t - t_1) V_2^*(t - t_2) \rangle \quad \textbf{(3-10)}$$

For a stationary, and ergodic process, we can say

$$I(\tau) = I_1 + I_2 + 2Re[\Gamma(\tau)] \quad \textbf{(3-11)}$$

where $I_1$and I_2 are the field intensities independent of time and Γ depends upon τ ,where $\tau = t_1 - t_2$ which is the time difference between the two paths. $\Gamma(\tau)$ stands as the field autocorrelation function for identical fields on the two arms. The complex degree of coherence can be defined as the normalized $\Gamma(\tau)$ as:

$$\gamma(\tau) = \frac{\Gamma(\tau)}{\Gamma(0)} = \frac{\Gamma(\tau)}{\sqrt{I_1 \cdot I_2}} \quad \textbf{(3-12)}$$

In which for the two fields being non-coherent $\gamma(\tau) = 0$, and for partially coherent waves $0 < \gamma(\tau) < 1$. γ is a parameter that represents the quality of the interference pattern. This parameter reveals the time delay in which case the interference can happen. For our measurements, we need to measure the distances in the order of several microns which translates to very small temporal delays. A broadband light source provides the coherence properties required for such measurements. This can effectively resolve the multiple light scattering.

3.2. Optical path-length spectroscopy

Low-coherence interferometry by using OPS is a commonly used method for different applications. It enables the possibility of characterizing the positions of optical reflections in the medium in a similar manner to OCT. The advantage of using a low-coherence source is to increase the resolution of the detected signal and to obtain better dynamic range [5]. This is because the interference between the two arms is observed only for backscattered light that

has traveled a distance equivalent to twice the reference arm length, which is adjusted by a scanning mirror. Having a low-coherence source helps to perform more precise depth-resolved measurements, this is because when the optical path difference in two arms is less than the coherence length of the source, the backscattered light can interfere with the reference.

This methodology has been used for characterizing optical properties of biological tissues non-invasively [18, 19]. The experimental setup for LCI based OPS shown in Figure 3-2. This geometry includes a fiber-based Michelson interferometer with a super luminescent diode (SLD). The broad band light source is divided into two arms by the beam splitter. In one arm the single mode fiber shines light on the sample and also collects the backscattered light. The other fiber is aligned to a reference mirror which is adjusted to compensate the optical path-length inside the sample. The two beams are recombined and the interference signal is formed on the detector. This method follows the principles of the time-resolved reflectance measurements and directly provides us the path-length distribution, $P(s)$.

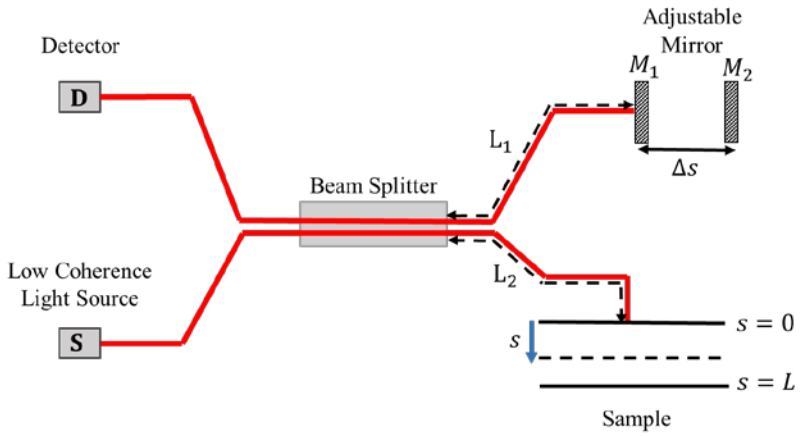

Figure 3-2 Experimental setup for a LCI based backscattering OPS

The intensity of the detected signal with the assumption of quasi-monochromatic optical fields ($\Delta\lambda/\lambda \ll 1$) can be written as following

$$I_d = I_{ref} + I_s + 2\sqrt{I_s}\sqrt{I_{ref}}\frac{\cos 2\pi\,\Delta s}{\lambda} \quad \textbf{(3-13)}$$

where I_d is the intensity of the detected signal, I_{ref} is the intensity of light in the reference arm, I_s is the intensity of the backscattered light from the sample, Δs is the path-length difference between the two arms, and λ is the wavelength of the light source. For two beams to interfere constructively, Δs must be a multiple of wavelength of the light source and also $|\Delta s|$ must be smaller than the coherence length of the light source l_c [5]. For the portion of the wave that is transported into a diffusive scattering medium, the optical path-length probability density, $P(s)$, describes the probability that the wave traveled for an optical-path length of s [5]. Practically, it is not possible to calculate $P(s)$ analytically. Therefore, we used the optical path-length spectroscopy to find $P(s)$ directly. The light-matter interaction with multiple scattering medium shows a property which is called enhanced coherent backscattering. This enhancement is originated from the in-phase interference of the backscattered light and will be enhanced comparing to the background light. OPS requires a backscattering geometry due to its coherent enhancement and ability to detect the $P(s)$ within the diffuse background. This is because the constructive interference in the backscattered direction boosts the signal.

A typical signal obtained from OPS measurements is shown in Figure 3-3. The path length distribution of light versus the optical path length is measured by adjusting the scanning mirror and recording the envelope of the interferogram for a backscattering light from a

multiple scattering medium. The signal for the backscattered light is the path-length resolved signal divided to the area under the curve. The signal reveals that as photons travel longer optical path-lengths, the signal drops more. By investigating the power-law decay and the amplitude of the recorded optical path-length probability distribution, we can study the properties of emerging radiation which depends on the geometry of the scattering medium.

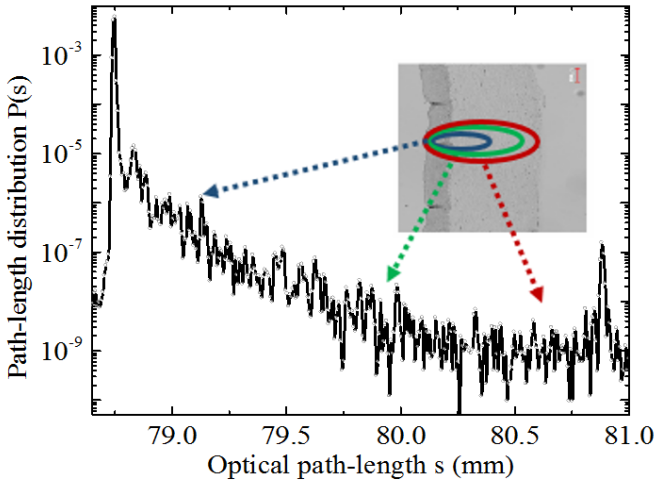

Figure 3-3 Measured path-length distribution vs optical path-length by using OPS method

We will present the experimental detail of the LCI based OPS measurements on the three-dimensional organotypic models of esophageal cell invasion by studying the optical path-length distribution of the backscattered light in normal and invasive conditions. Main goal is to monitor the effect of the extracellular matrix on the invasiveness of the esophageal tissues as well as the induction of signaling pathways. In this work, we used a precision Reflectometer instrument (Hewlett-Packard Model HP 8504B) working with single mode optical fibers and based on Michelson interferometry configuration. The experimental conditions and results will be presented in the next chapter.

CHAPTER 4: EXPERIMENTS ON AN IN-VITRO MODEL SYSTEM OF ESOPHAGUS TISSUE

In this chapter, we present OPS measurements with a low-coherent source on an *in-vitro* model system of esophagus tissues to study the properties of backscattered light. This optical sensing method attains a better understanding from the interaction of light with tumor invasion and structural changes in extracellular matrix associated with the invasion of tumor cells. Next section, introduces the important parameters affecting the invasiveness of the esophageal tissues.

4.1. Model system of Esophageal tissues

Esophageal cancer (EC) is known as one of the most common types of cancer in the world, the 6th leading reason of cancer death, and the 8th most frequent cancer worldwide [20]. About 17,000 adult including 13,500 men and 3,500 women are suffering from esophageal cancer and surprisingly EC mortality rate for 2016 is reported to be around 16,000 [21]. In men, with an average age above 67 years old, the threat of developing esophageal cancer is relatively higher [22]. There are two main cases of esophageal cancer including esophageal squamous cell carcinoma (ESCC) and esophageal adenocarcinoma (EAC). According to studies on 22,123 patients suffering from esophageal cancer, 8156 (~37%) patients are diagnosed with squamous cell carcinoma, 13814 (~62%) with adenocarcinoma, 116 (less than 1%) with adenosquamous carcinoma, and the remaining 37 with undifferentiated carcinoma [23]. The rate of adenocarcinoma is increasing in Western countries [24]. The impact of obesity, gastroesophageal reflux, and Barret's epithelium which arises as a result of lifestyle changes and diet, increases rates of EAC in these countries [21]. Other factors such as age, gender, and

smoking tobacco also promotes the risk of this cancer [25]. While the progression of EAC is reflected by the metaplasia of the esophageal squamous lining to a columnar glandular phenotype, squamous cell carcinoma (SCC) retains the morphology and the characteristics of the esophageal inner lining. The squamous cell carcinoma esophageal cancer is the highest in east Asia, east and south of Africa, and some areas in Europe which has been reduced during previous three decades [26]. On the contrary, in middle east and south Africa, SCC in esophagus, head, and neck is high because of using tobacco and alcohol consumption [21]. Nutritional deficiency such as lack of Zinc, Folate, Selenium, Vitamin A, E, and C is another important factor that increases the risk of ESCC in developing countries [27]. Dysphagia (difficulty in swallowing), weight loss, and chest pain are the common symptoms of the two main types of esophageal cancer.

Accumulation of abnormal cells causes formation of a tumor in esophagus. The tumor microenvironment contributes to cell invasion through reorganization of the extracellular matrix and induction of signaling pathways. According to recent studies, the stiffness of matrix is related with tumor progression; for instance, the stiffness of matrix promotes the tumorigenesis in breast cancer [28]. Besides providing structural support to the surrounding cells, which is playing role in the extracellular matrix, it also plays significant role in regulations of cell growth [29]. Intercellular Communication (IC) is another critical factor that may improve or prevent development of esophageal cancer. The Transforming Growth Factor β (TGFβ) signaling pathway is a form of intercellular communication which plays a vital role in the regulation of cell growth, cell proliferation, cell differentiation, and apoptosis. The TGF β signaling process is initiated from binding of TGF β superfamily ligands to TGFβ type II

receptor, then recruiting a TGF β type I receptor to form a hetero-tetrameric. The binding results in a conformational change in the heterotetrameric complex, and hence phosphorylation of serine residues of type I receptor by type II receptor. Receptor-regulated SMADs (R-SMADs) are transcription factors which includes SMAD2 and SMAD3 that undergoes transduction of extracellular signals of the TGF β superfamily ligands from the cell cytoplasm to the nucleus. The activated heterotetrameric complex phosphorylates the R-SMADs, and they bind together because of the high affinity of R-SMADs to coSMAD (SMAD 4). The activated complex of RSMADs-coSMAD travels into the nucleus of the cell and binds to the promoter region of DNA in the transcription process of mRNA. In Figure 4-1, the TGFβ signaling pathway is shown in cellular membrane and nuclear membrane.

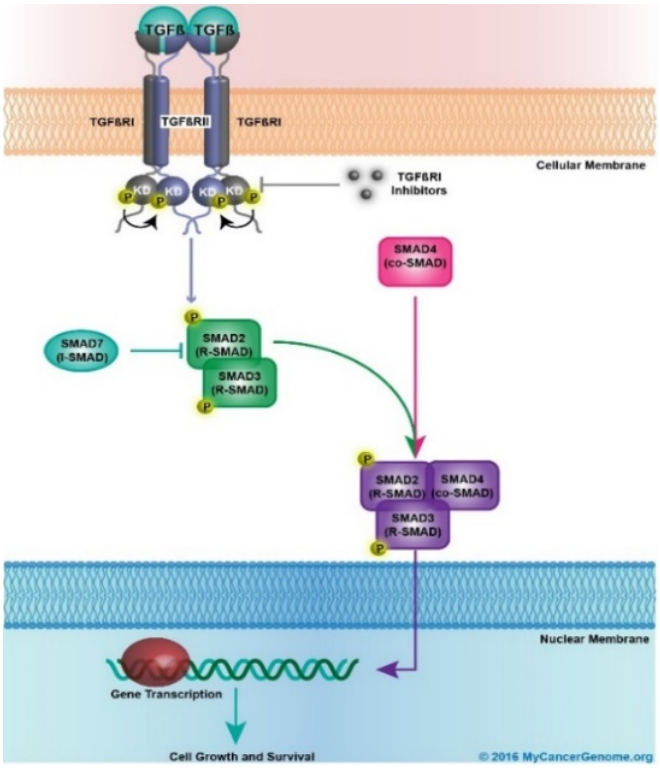

Figure 4-1 The transforming growth factor β (TGFβ) signaling pathway [30]

Therefore, the inhibition of TGFβ signaling pathway in normal cells initiates tumorigenesis of squamous cell carcinoma. A83-01 is used as an inhibitor of TGF β type I receptor [31]. Figure 4-2 shows the molecular structure of A83-01 ($C_{25}H_{19}N_5S$) whit 21.52 g/mol molecular weight. This compound prevents phosphorylation of SMAD2, suppresses TGFβ signaling, and increases the invasiveness consequently.

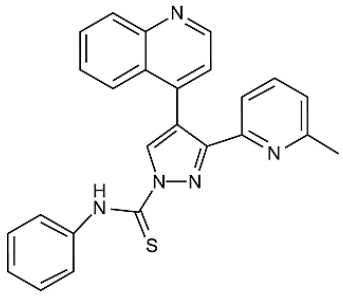

Figure 4-2 Molecular structuer of A83-01[30]

Dr. Andl's laboratory found that increasing the concentration of collagen might improve the stiffness of a matrix and thus results in reduction of invasiveness. However, in the presence of TGFβ inhibitor, the high concentration of matrix does not prevent the tumor progression [32]. In Figure 4-3, it is shown that how matrix density is related to the degree of invasiveness in the presence or absence of TGFβR inhibitor. In a collaborative research, we non-invasively used our OPS technique to study the changes in optical properties to monitor the effects of the mentioned parameters in the invasiveness of the tissues.

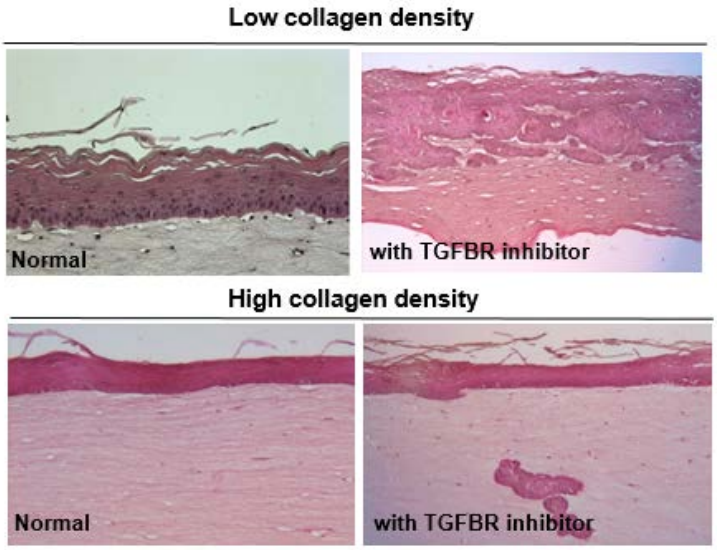

Figure 4-3 Effect of TGFβR inhibitor in a normal tissue and high colagen density tissue (from Andl Lab in the Burnett School of Biomedical Science at the University of Central Florida)

4.2. Precision Reflectometry

In this work, we used a precision reflectometer (Hewlett-Packard Model HP 8504B) working based on Michelson interferometer to measure the backscattered light. This instrument records the return loss which is the ration of the collected backscattered light to the input power. The HP 8504B precision Reflectometer can be used with either single-mode or multi-mode optical fibers for the wavelength range of 1300nm to 1550 nm [33]. In this work, we used an external 1310 nm super-luminescent diode and single-mode optical fibers.

The reflectometer instrument has two sections: 1) Lightwave system and 2) display processor as shown in Figure 4-4. Each time, the instrument needs to be calibrated before making any measurements. This means that the two arms of the Michelson interferometer have to be approximately equalized. First, the reference extension fiber and a low-reflection termination load (>40 dB) (1 in Figure 4-4) has to be connected to the ports of the device. The

calibration process will remove the DC offsets and polarization sensitivity by adjusting the reference polarization balance knobs. Second, a fiber with almost same length with known return loss has to be used to measure the standard.

After finishing the calibration, a cleaved single-mode optical fiber is used to the inject the light into the sample and collect the backscattered power. A micrometer motion controller (EPS300 Motion Controller/Driver by Newport) is used to control 3-axis micrometer stage in order to control where the tip of the fiber touches the surface of the sample and to perform raster scanning.

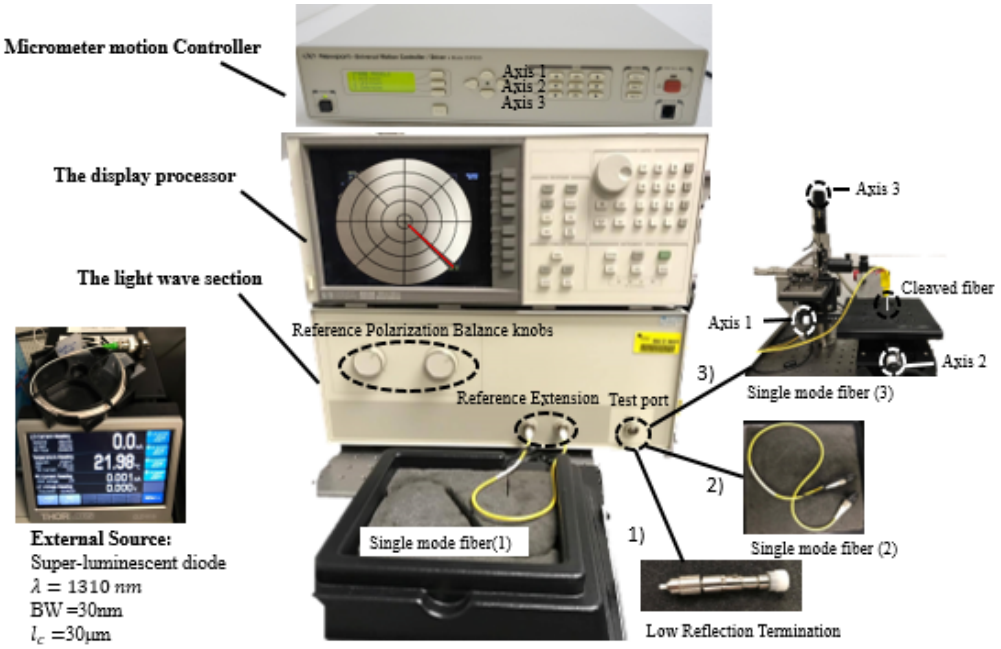

Figure 4-4 Agilent HP 8504B 1300-1550 nm precision reflectometer

Optical fibers are usually made of five layers as shown in Figure 4-5. The outer layer or the cable jacket is a yellow plastic protective cover with a diameter of $\sim 400\ \mu m$. The second outer layer is called buffer which is made from yellow strings to strength the fiber. The coating layer is a white plastic coating for protecting the cladding layer with a diameter of $\sim 250\ \mu m$.

The core ($\sim 8.5\ \mu m$) is the innermost glass layer covered by the cladding layer ($\sim 125\ \mu m$) and lower index than cladding to make the total internal reflection possible.

For our measurements, the tip of the fiber needs to be cleaned and precisely cleaved. The angled cleavage of the tip increases the loss and noises. First, the outer cable jacket is stripped with the fiber stripping hand tool. After cutting the buffer, and removing the coating layer, the cladding layer needs to be removed generously with a wire stripper. Finally, the core has to be cleaned with isopropyl alcohol (IPA), and cleaved with a mechanical cleaver as shown in Figure 4-5 Layers of an optical fiber, tools for cleaving process

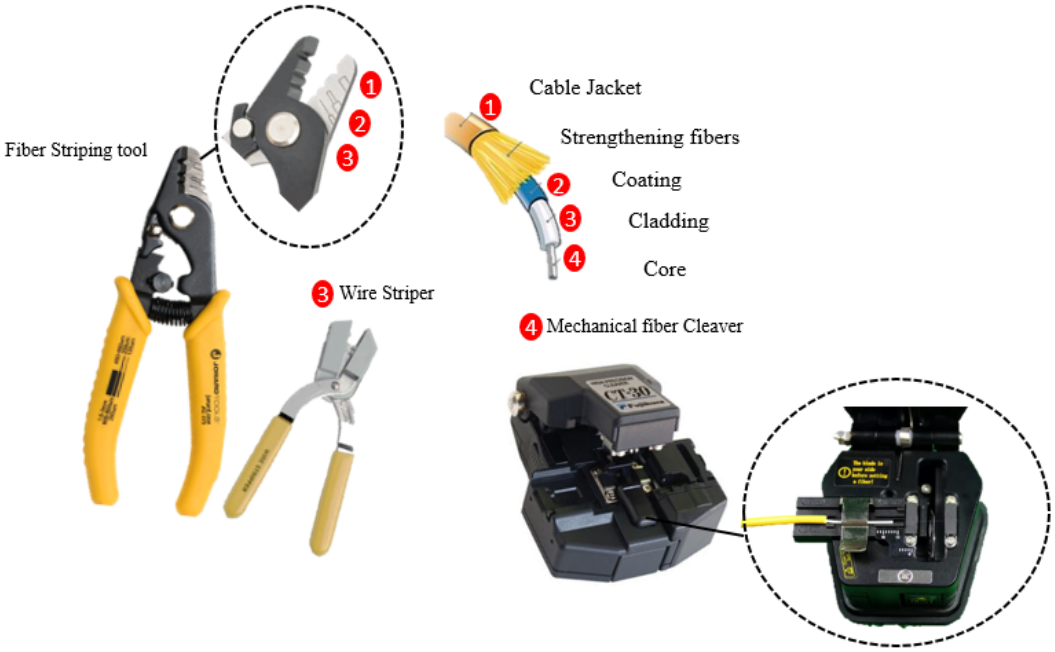

Figure 4-5 Layers of an optical fiber, tools for cleaving process

In this work, we used an external high power super-luminescent light source at 1310 nm, with a bandwidth of 30 nm, and coherence length of $l_c = 30\mu m$. A DC power supply (GwInstek GPT-3060D) was used to drive the source and the cooling fan.

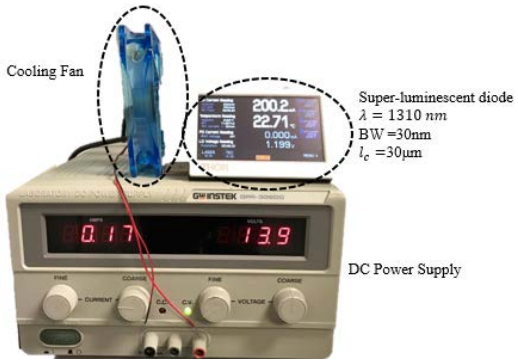

Figure 4-6 DC power supply and light source controller

4.2.1. Experiments on esophageal tissue samples

We performed path-length spectroscopy measurements on organotypic esophageal tissue samples. The reflectometer gives the optical interferogram in which case displays the distribution of optical path-length that a photon may have traveled inside the organotypic esophageal tissue denoted by $p(s)$. The experimental conditions are shown in the figure below:

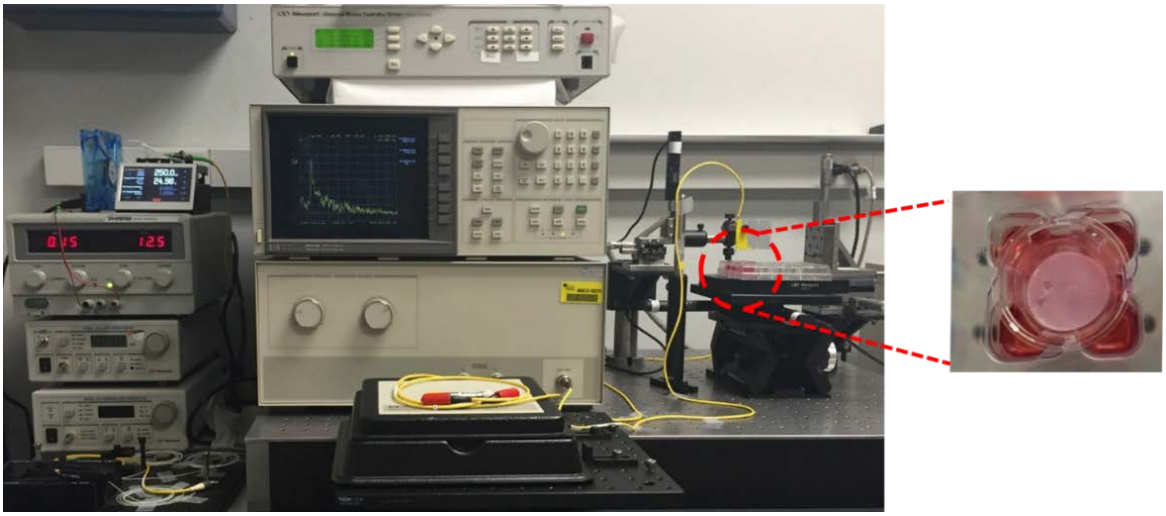

Figure 4-7 Esophageal tissue samples and the reflectometer instrument, OPS measurements were performed with single mode optical fibers

When the single mode fiber is placed approximately $100\mu m$ far from the sample, the OPS signal shows different peaks. The first peak is generated as a result of the interference between the two arms (backscattered light and the reference arm). The second peak represents the shortest path (s_1) that photons have traveled and indicates the presence of a layer which corresponds to the epithelium layer. The third peak demonstrates the longest path (s_2) that photons have traveled which specifies the presence of the membrane as shown in the Figure 4-8:

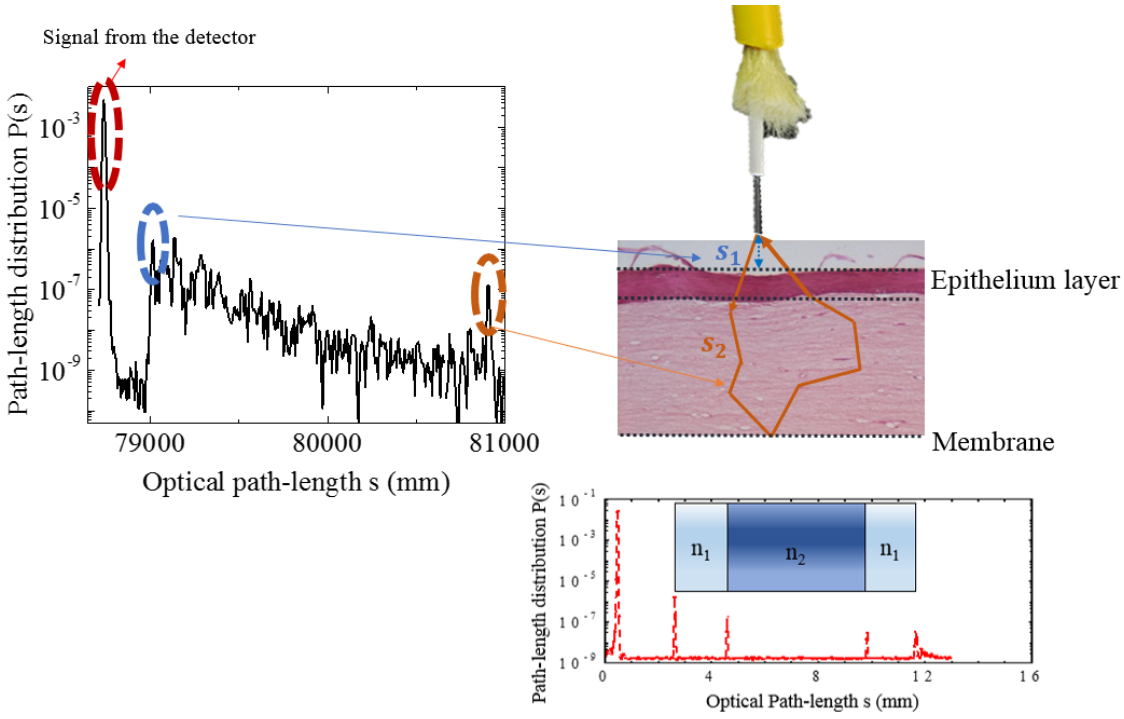

Figure 4-8 The preliminary signal observed from the sample

By moving the single-mode optical fiber closer to the surface, and by controlling the vertical micrometer stage, the first and second peaks will be on top of each other in which case shows the position where the fiber tip touches the epithelium layer.

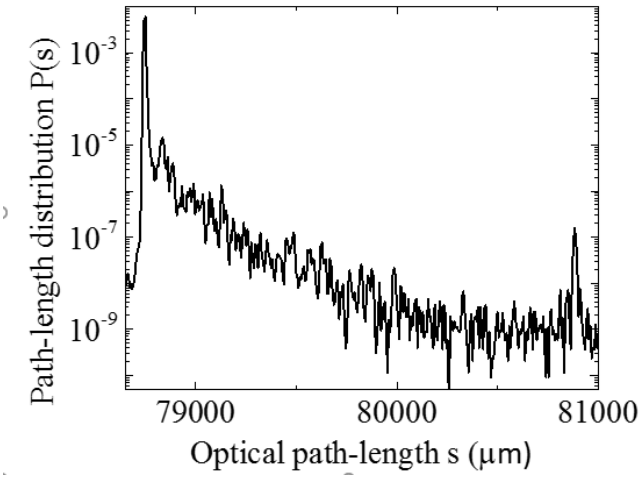

Figure 4-9 The measured OPS signal when the fiber tip is touching the epithelium layer

4.2.2. Results and discussions

As it was previously mentioned, lack of TGFβ signaling stimulates the invasion in the cellular matrix embedded with fibroblasts and an epithelium layer (the top layer) [32]. Also, the stiffness of a matrix composed of matrix gel and collagen results in prevention of invasiveness although the epithelial cells that are used are naturally invasive due to the genetic modification that are intentionally made on the cells. However, in presence of TGFβ inhibitor, the high concentration of collagen prevents the cell invasion, but not completely inhibit it. Therefore, the tumor progression is improved in the low collagen density of matrix. Dr. Andl's group provided us with a model system to monitor the effects of the mentioned parameters on invasiveness of the tissue. The general process for growing these models is depicted in Figure 4-10.

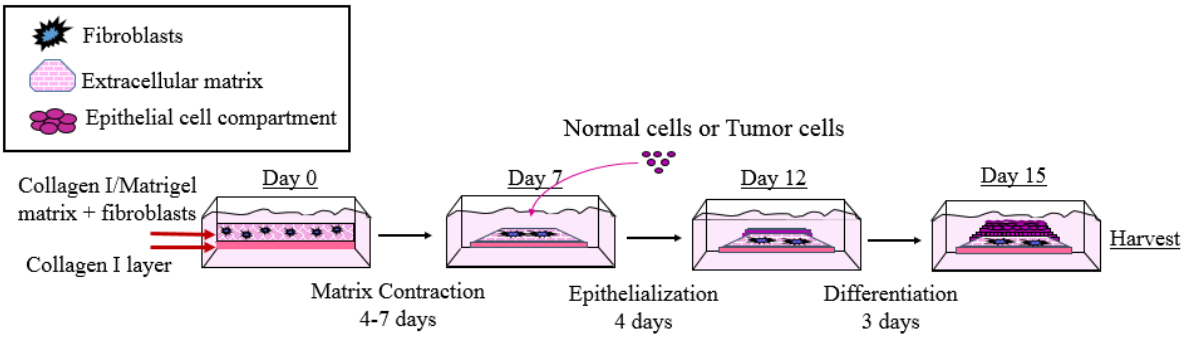

Figure 4-10 Protocol for growing the organotypic model systems (from Andl Lab in the Burnett School of Biomedical Science at the University of Central Florida)

First, we performed OPS measurements on a preliminary groups of sample, to investigate the ability of light to propagate into the gel (extracellular matrix) with a given concentration, and to study the backscattered light in the presence of fibroblasts (type of cell that generally deposits and crosslinks the extracellular matrix proteins) or the epithelium layer. We observed consistency in few initial measurements which are shown below

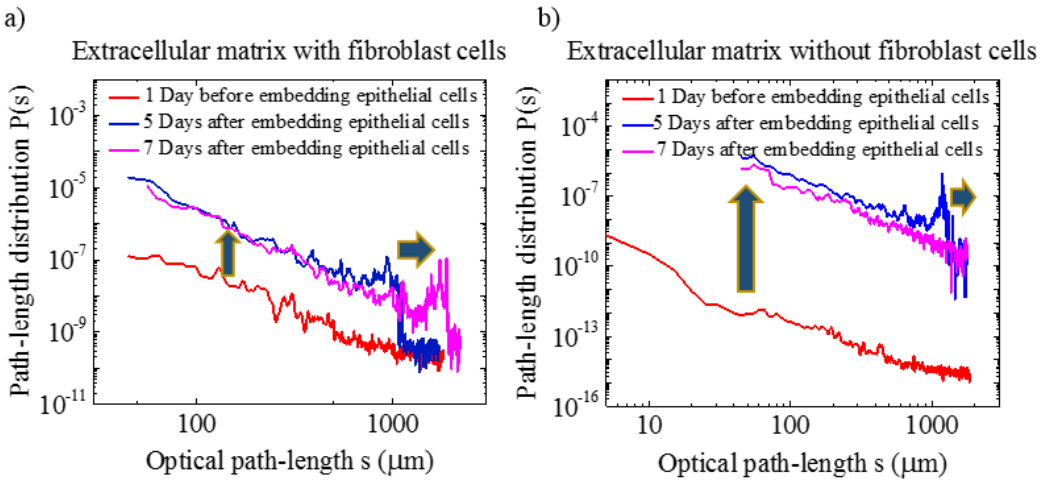

Figure 4-11 Measured path length distributions for cultures in normal condition in the presence and absence of fibroblasts in several days after embedding epithelial cells

The increase in the signal for the cases of cells with embedded epithelium shows the fact that the refractive index of the epithelial cells is higher comparing to the gel matrix. We also note that, the increase in the signal in Figure 4-11(a), which is the case with fibroblast cells, is less than Figure 4-11(b) where the extracellular matrix lacks fibroblast cells. Our time-dependent study reveals that the peak of the backscattered light from membrane is shifting to the longer optical path-lengths. This indicates that the epithelium layer has become more homogeneous, and subsequently this layer may prevent the light to escape. Also, we note that during the time, the gel medium becomes more condensed and thinner, therefore, the optical beam may have penetrated closer to the membrane medium.

The second set of measurements were performed on two different group of samples: 1) a tissue sample with a high collagen density matrix which resembles a low invasion, 2) a tissue sample after treatment with the TGFβR inhibitor on a high collagen density matrix which shows as a medium invasion. The Hematoxylin and Eosin (H&E) of two cultures are shown below.

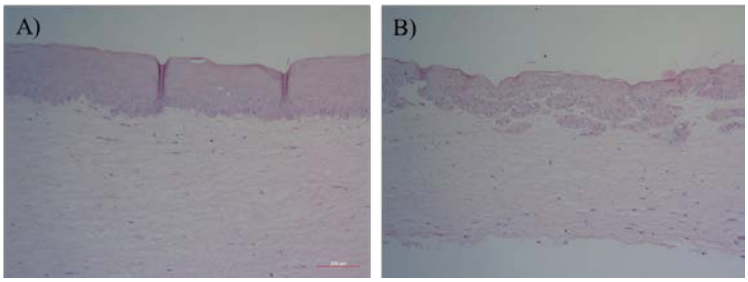

Figure 4-12 A) H&E of Cellular matrix with high collagen density in absence of TGFβR inhibitor (low invasion) B) H&E of Cellular matrix with high collagen density and TGFβR inhibitor (medium invasion), (from Andl Lab in the Burnett School of Biomedical Science at the University of Central Florida)

The optical path-length probability density for both samples are measured by using OPS technique in different days (4, 7, and 9 days after making the epithelial cells). These measurements were performed on each culture in 30 different locations with averaging factor of 75, 250 mA driving current, and with 4 mm span range. Figure 4-13 is the measured OPS signal for different samples shown in logarithmic scale in both axes.

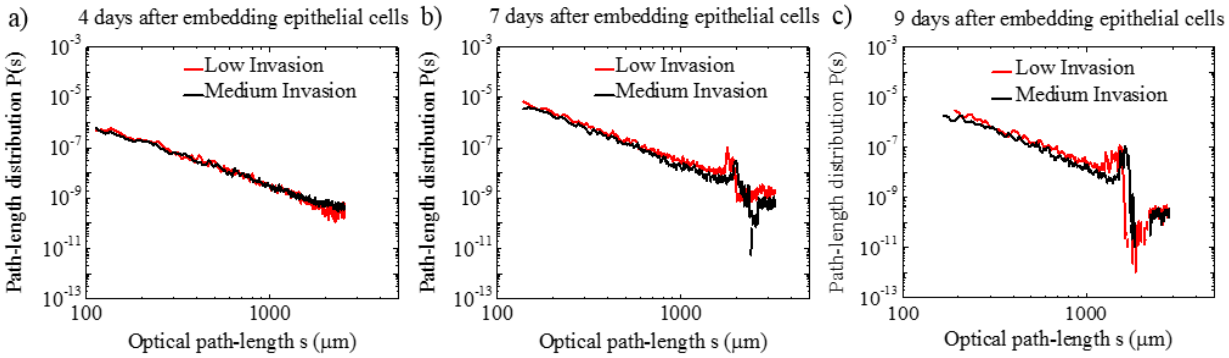

Figure 4-13 Measured $P(s)$ vs optical path-length (s) for low invasion, and medium invasion samples in logarithmic scales during different days (a) 4 days after embedding epithelial cells, (b) 7 days after embedding epithelial cells, and (c) 9 days after embedding epithelial cells

We observed that as the gel medium becomes more condense during the time, the peaks from the membrane become more pronounced as we have seen before. Since the OPS signal depends on the volume of interaction of light with samples, the area under the curves provides us the total reflection of light from the sample in which case we observed higher reflection for the low invasion condition. The measurements are done in different days to obtain more accurate observations and to monitor the evolution.

To fully characterize the effect of collagen density and TGFβ R inhibitor, we also performed OPS on another sample with low collagen density in its cellular matrix in absence

of TGFβ R inhibitor together with two newly prepared samples with same condition as before. The Hematoxylin and Eosin (H&E) of three organotypic cultures are shown below:

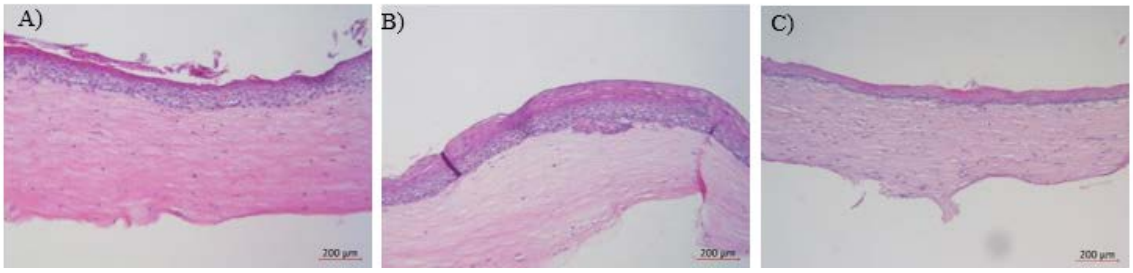

Figure 4-14 H&E of Cellular matrix with high collagen density in absence of TGFβR inhibitor (low invasion) B) H&E of Cellular matrix with high collagen density and TGFβR inhibitor (medium invasion) C) H&E of Cellular matrix with low collagen density in absence of TGFβR inhibitor (high invasion), (prepared in Andl's Lab in the Burnett School of Biomedical Science at the University of Central Florida)

We performed measurements on these samples before embedding the epithelial cells and 5, 7, 8, and 9 days after the embedding process to study the behavior during the time. The measurements were performed in 50 different locations with averaging factor of 30, 250 mA driving current, and 4 mm span range.

With reference to the measurement results Figure 4-15, the peaks are showing the longest path that photons have traveled which is from the lowest layer of the model system. We note that the path-length (s) where the peak from the low invasion culture occurs, remain constant. However, the peaks for the other two cultures occur at shorter path-lengths and shifts during the time. This time-dependent study shows that the high invasion sample shrinks with a higher rate than the medium invasion and low invasion samples. Comparing the area under the curves, we observed that the reflection from the samples varies in different conditions. The comparison of the reflection from each sample, shown in Table 4-1, may reveal more

information on the structural properties of each case. To understand this further, more precise measurements are required. Our preliminary measurements show that the reflection from the samples with low invasion condition is the highest. This may be because of the less scattering events in this condition.

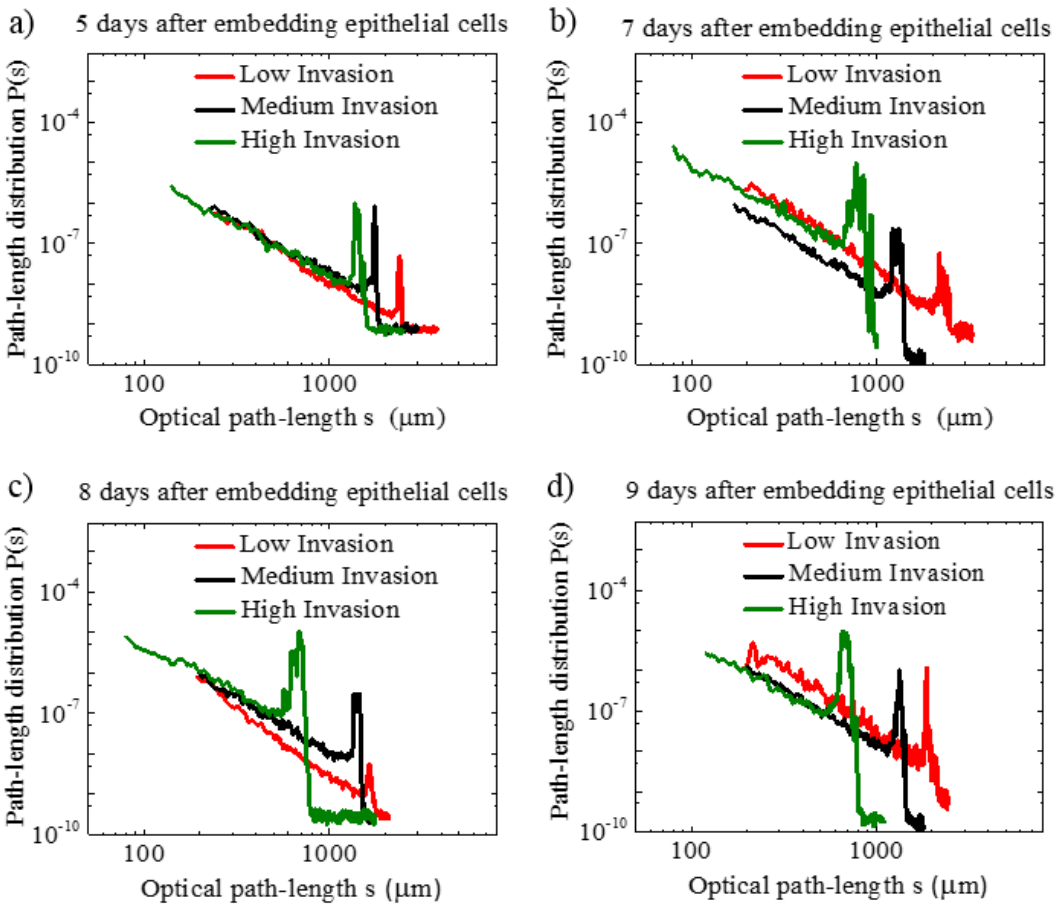

Figure 4-15 OPS measurements on low invasion, medium invasion, and high invasion in different days, (a) 5 days after embedding epithelial cells, (b) 7 days after embedding epithelial cells, (c) 8 days after embedding epithelial cells, (d) 9 days after embedding epithelial cells

Table 4-1 Area Under the graph from 10 μm to 500μm ($\times 10^{-4}$)

After embedding epithelium	5 days	7 days	8 days	9 days
Low Invasion	13	14	*6.6	7.7
High Invasion	6.4	4.8	6.5	5.3
Medium Invasion	6.1	2.9	3.5	3.7

*Normal sample was contaminated after day 8.

By investigating the power-law exponent decay of the signals in logarithmic scale Figure 4-16, we studied the diffusive behavior of our samples. For the samples in low invasion condition, we note that the signal decayed with an exponent smaller than $-5/2$ which means that the propagation has not reached to the normal diffusive regime and it may be due to the less scattering events happening in the sample. We observed that the signal for medium and high invasion samples, the decay follows the $-5/2$ and corresponds to the normal diffusive regimes. Therefore, more scattering events are occurring in these two cases.

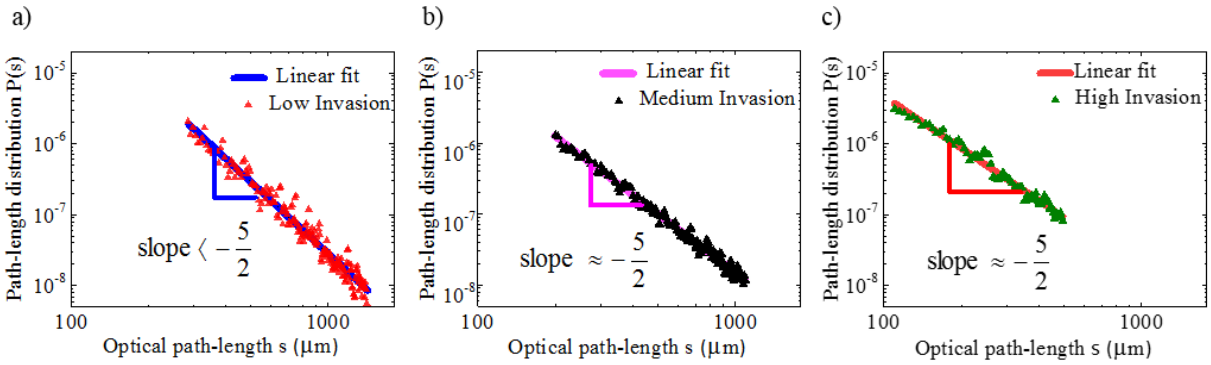

Figure 4-16 Averaged measurements on 50 different points on the sample for three different conditions, (a) Low Invasion, (b) Medium Invasion, (c) High Invasion, shown in logarithmic scales with a linear fit

Based on our observations, we can conclude that the structure of the samples is as below

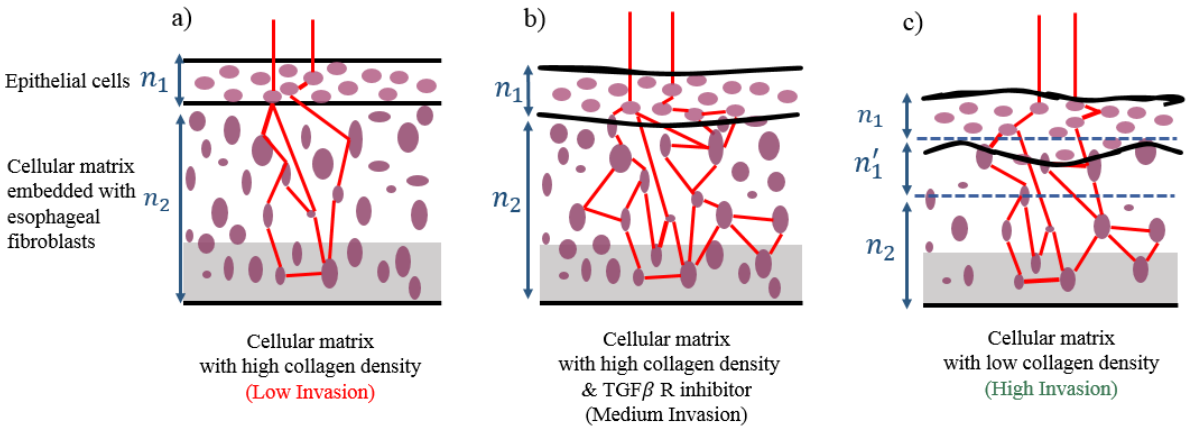

Figure 4-17 Structural properties of investigated three different conditions

CHAPTER 5: CONCLUSIONS

In this thesis we report experimental investigations on the scattering properties of three different model systems of Esophageal tissues. The results were obtained using the OPS technique based on low-coherent interferometry. This technique permits non-invasive monitoring of the evolution of tissue invasion. We observed that different conditions of Esophageal tissues affect differently on the backscattered light. This methodology can provide averaged information about the nature of interaction between light and inhomogeneous materials and subsequently reveal unique structural fingerprints of the complex medium. We have also demonstrated the capability of this method to follow the structural changes for in tissues samples during a two-week period.

LIST OF REFERENCES

1. Hariharan, P., *Optical interferometry*. 2003: Academic press.
2. Goodman, J.W., *Some fundamental properties of speckle.* JOSA, 1976. **66**(11): p. 1145-1150.
3. Alarousu, E., et al., *Study on the use of optical coherence tomography in measurements of paper properties.* Measurement Science and Technology, 2005. **16**(5): p. 1131.
4. Carlsson, J., et al., *Time-resolved studies of light propagation in paper.* Applied optics, 1995. **34**(9): p. 1528-1535.
5. Popescu, G. and A. Dogariu, *Optical path-length spectroscopy of wave propagation in random media.* Optics letters, 1999. **24**(7): p. 442-444.
6. Wiersma, D.S., *Disordered photonics.* Nature Photonics, 2013. **7**(3): p. 188-196.
7. *Radiative transfer. By S. Chandrasekhar. London (Oxford University Press) 1950. 8vo. Pp. 393, 35 figures. 35s.* Quarterly Journal of the Royal Meteorological Society, 1950. **76**(330): p. 498-498.
8. Patterson, M.S., B. Chance, and B.C. Wilson, *Time resolved reflectance and transmittance for the noninvasive measurement of tissue optical properties.* Applied optics, 1989. **28**(12): p. 2331-2336.
9. Ishimaru, A., *Wave propagation and scattering in random media*. Vol. 2. 1978: Academic press New York.
10. Naraghi, R.R. and A. Dogariu, *Phase Transitions in Diffusion of Light.* Physical Review Letters, 2016. **117**(26): p. 263901.

11. Naraghi, R.R., et al., *Near-field effects in mesoscopic light transport.* Physical review letters, 2015. **115**(20): p. 203903.

12. Tearney, G.J., et al., *In vivo endoscopic optical biopsy with optical coherence tomography.* Science, 1997. **276**(5321): p. 2037-2039.

13. Fujimoto, J.G., et al., *Optical coherence tomography: an emerging technology for biomedical imaging and optical biopsy.* Neoplasia, 2000. **2**(1-2): p. 9-25.

14. Michelson, A.A. and E.W. Morley, *On the Relative Motion of the Earth and of the Luminiferous Ether.* Sidereal Messenger, vol. 6, pp. 306-310, 1887. **6**: p. 306-310.

15. Menzies, A., *Frank Twyman. 1876-1959.* Biographical Memoirs of Fellows of the Royal Society, 1960. **5**: p. 269-279.

16. Brown, R.H. and R. Twiss, *A test of a new type of stellar interferometer on Sirius.* Nature, 1956. **178**(4541): p. 1046-1048.

17. Abbott, B.P., et al., *Observation of gravitational waves from a binary black hole merger.* Physical review letters, 2016. **116**(6): p. 061102.

18. Schmitt, J., A. Knüttel, and R. Bonner, *Measurement of optical properties of biological tissues by low-coherence reflectometry.* Applied Optics, 1993. **32**(30): p. 6032-6042.

19. Zhu, Y., N.G. Terry, and A. Wax, *Angle-resolved low-coherence interferometry: an optical biopsy technique for clinical detection of dysplasia in Barrett's esophagus.* Expert review of gastroenterology & hepatology, 2012. **6**(1): p. 37-41.

20. Pennathur, A., et al., *Oesophageal carcinoma.* The Lancet, 2013. **381**(9864): p. 400-412.

21. Le Bras, G.F., et al., *Esophageal cancer: The latest on chemoprevention and state of the art therapies.* Pharmacological research, 2016. **113**: p. 236-244.

22. Enzinger, P.C. and R.J. Mayer, *Esophageal cancer.* New England Journal of Medicine, 2003. **349**(23): p. 2241-2252.

23. Rice, T., et al., *Worldwide Esophageal Cancer Collaboration: clinical staging data.* Diseases of the Esophagus, 2016. **29**(7): p. 707-714.

24. Rubenstein, J.H. and N.J. Shaheen, *Epidemiology, diagnosis, and management of esophageal adenocarcinoma.* Gastroenterology, 2015. **149**(2): p. 302-317. e1.

25. Falk, G.W., *Barrett's oesophagus: Frequency and prediction of dysplasia and cancer.* Best Practice & Research Clinical Gastroenterology, 2015. **29**(1): p. 125-138.

26. Pickens, A. and M.B. Orringer, *Geographical distribution and racial disparity in esophageal cancer.* The Annals of thoracic surgery, 2003. **76**(4): p. S1367-S1369.

27. Limburg, P.J. and D.A. Dixon, *Gastrointestinal Neoplasia.* Gastroenterology Clinics. **45**(3): p. i.

28. Provenzano, P.P., et al., *Collagen density promotes mammary tumor initiation and progression.* BMC medicine, 2008. **6**(1): p. 11.

29. Chou, E.Y., *Understanding the patterned deposition of lignin in secondary cell walls*. 2017, University of British Columbia.

30. Rastgar Jazii, F., *Esophageal cancer-cell and molecular biology, biomarkers, nutrition and treatment.* Janeza Trdine 9, 51000 Rijeka, Croatia, 2012. **254**.

31. *A83-01, ALK5 Inhibitor, A8301 Small Molecule - ESI BIO*. 2017; Available from: http://www.esibio.com/a8301/.

32. Le Bras, G.F., et al., *TGFβ loss activates ADAMTS-1-mediated EGF-dependent invasion in a model of esophageal cell invasion.* Experimental cell research, 2015. **330**(1): p. 29-42.

33. Braun, D.M., et al., *Precision Reflectometer with Spurious-Free Enhanced Sensitivity.* HEWLETT PACKARD JOURNAL, 1995. **46**: p. 39-39.